



Visible-light-driven photodegradation of acetaldehyde gas catalyzed by aluminosilicate nanotubes and Cu(II)-grafted TiO₂ composites



Ken-ichi Katsumata^{a,b,*}, Xiao Hou^{a,b}, Munetoshi Sakai^b, Akira Nakajima^{b,c}, Akira Fujishima^{b,d}, Nobuhiro Matsushita^a, Kenneth J.D. MacKenzie^e, Kiyoshi Okada^a

^a Materials and Structures Laboratory, Tokyo Institute of Technology, 4259 Nagatsuta, Midori, Yokohama, Kanagawa 226-8503, Japan

^b Photocatalyst Group, Kanagawa Academy of Science and Technology, 3-2-1 Sakado, Takatsu, Kawasaki, Kanagawa 213-0012, Japan

^c Department of Metallurgy and Ceramics Science, Tokyo Institute of Technology, 2-12-1 O-okayama, Meguro, Tokyo 152-8552, Japan

^d Research Institute for Science and Technology, Energy and Environment Photocatalyst Research Division, Tokyo University of Science, 1-3 Kagurazaka, Shinjuku, Tokyo 162-8601, Japan

^e MacDiarmid Institute for Advanced Materials and Nanotechnology, Victoria University of Wellington, PO Box 600, Wellington, New Zealand

ARTICLE INFO

Article history:

Received 13 November 2012

Received in revised form 23 February 2013

Accepted 1 March 2013

Available online 14 March 2013

Keywords:

Imogolite

TiO₂

Photocatalyst

Relative humidity

Interfacial charge transfer

Acetaldehyde

ABSTRACT

Aluminosilicate nanotubes and Cu(II)-grafted TiO₂ composites were prepared, and the acetaldehyde degradation activity of the composites was evaluated at various relative humidities. The aluminosilicate nanotubes were synthesized hydrothermally and characterized by TEM, XRD, ²⁷Al and ²⁹Si NMR, FT-IR, N₂ and water vapor isotherms. Their morphology was nanotubular with 3–5 nm outer diameter, and the specific surface area was 245 m²/g. The aluminosilicate had a strong affinity for water molecules, and the structure was determined to be an imogolite by ²⁷Al and ²⁹Si NMR. TiO₂ and imogolite composites exhibited higher activity for the photodegradation of acetaldehyde under UV irradiation than TiO₂, but was dependent on the relative humidity. Cu(II)-grafted TiO₂ and imogolite composites exhibited higher activity for the photodegradation of acetaldehyde under visible light irradiation than Cu(II)-grafted TiO₂, and were less affected by the relative humidity. These results show that Cu(II)-grafted TiO₂ - imogolite composites exhibit very efficient absorption and photodecomposition of acetaldehyde in a variety of environments.

© 2013 Elsevier B.V. All rights reserved.

1. Introduction

Volatile organic compounds (VOCs) are typical air pollutants mainly emitted from industrial processes and transport vehicles. These cause various environmental problems and have adverse effects on human beings. The removal method of VOCs from air has been attempted using physical, chemical, and biological techniques [1–3], of which activated carbon adsorption is the most widely studied and used [4–10]. However, this method simply transfers organics from the gas to the solid phase, and increases the environmental load because of the need to dispose of the activated carbon containing adsorbed VOCs. A method which can completely decompose or remove VOCs is needed.

Titanium dioxide (TiO₂) is a well-known efficient photocatalyst [11]. TiO₂ is activated by irradiation with ultraviolet (UV) light, generating electron-hole pairs which reduce and oxidize adsorbates on

the surface, thereby producing radical species, such as OH radicals and O₂[−]. These radicals are strong oxidizing agents and can decompose most organic compounds [12–17] and bacteria [18–22]. Many studies have been conducted on the application of TiO₂ to water [23–25] and air purification [26–33] because TiO₂ has not only an excellent photocatalytic activity but is also highly chemically stable, non-toxic and inexpensive. However, since the concentration of pollutants in air is quite low, the efficiency of the photocatalytic activity is very low due to its small specific surface area and low adsorption ability.

Clays have been used in combination with TiO₂ photocatalyst to enhance the removal of organic pollutants. Clay-TiO₂ composites have been studied as photocatalytic materials with good absorption ability [34–44]. Ménési et al. [41] reported that VOCs are degraded at a significantly higher efficiency on TiO₂/Ca-montmorillonite composites than on pure TiO₂. Kameshima et al. [43] reported that the photocatalytic decomposition of 1,4-dioxane by TiO₂/montmorillonite composites was more efficient than for pure anatase (TiO₂) due to the synergy effect of adsorption for 1,4-dioxane and photodecomposed intermediates by montmorillonite and its photodecomposition by TiO₂. Kabanova et al. [44]

* Corresponding author at: Materials and Structures Laboratory, Tokyo Institute of Technology. Tel.: +81 45 924 5323; fax: +81 45 924 5358.

E-mail address: katsumata.k.ab@m.titech.ac.jp (K.-i. Katsumata).

also reported that synthetic hectorite-TiO₂ composites favored the adsorption and enhanced the photocatalytic degradation of VOCs. The photocatalytic activity of kaolinite-TiO₂ composites formed by deposition of TiO₂ on the external surface of kaolinite, was also enhanced. Thus, clay-supported TiO₂ photocatalysts can potentially improve the performance of air treatment techniques because of enhanced adsorption and reactivity of the target VOCs.

Imogolite is an aluminosilicate with a single-walled nanotubular structure consisting of a layer of aluminum(III) hydroxide (gibbsite), with isolated silicate groups bound on the inner wall [45]. The synthesis and properties of imogolite have been investigated over many years [45–48], and imogolite nanotubes have also been investigated for use as a catalyst support [49], methane storage [50,51], and as heat exchange materials [52]. Imogolite is expected to be a superior absorbent due to its large specific surface area arising from its nanotubular structure. However, the removal and photodegradation of VOCs using imogolite-TiO₂ composites has not been investigated.

The present is focused on imogolite which exhibits high photocatalytic activity under visible light irradiation [53], and Cu(II)-grafted TiO₂, which is an absorbent and visible-light-driven photocatalyst [54]. The imogolite was synthesized by a hydrothermal method, and the removal and photodegradation activity of acetaldehyde gas by imogolite and TiO₂ or Cu(II)-grafted TiO₂ composites was evaluated at various relative humidity condition under UV and fluorescent light irradiation.

2. Experimental

2.1. Materials

Tetrasodium silicate *n*-hydrate ($2\text{Na}_2\text{O}\cdot\text{SiO}_2\cdot n\text{H}_2\text{O}$), aluminum nitrate nonahydrate ($\text{Al}(\text{NO}_3)_3\cdot 9\text{H}_2\text{O}$, 99.9%), nitric acid (HNO_3 , 65%), ammonia solution (NH_4OH , 28%), copper(II) chloride dihydrate ($\text{CuCl}_2\cdot 2\text{H}_2\text{O}$, 99.9%), titanium(IV) oxide powder (rutile form, TiO₂, grain size 5 μm, 99.9%) were purchased from Wako Pure Chemical Industries, Tokyo, Japan. Water was purified by using a Millipore installation.

2.2. Synthesis of Imogolite

Imogolite powder samples were synthesized by the hydrothermal method shown in Fig. 1. Tetrasodium silicate *n*-hydrate solution (0.10 mol/L) and aluminum nitrate nonahydrate solution (0.25 mol/L) were mixed in a Si/Al = 0.4 molar ratio. After stirring for 90 min, 28% ammonia solution was slowly added and the solution stirred vigorously to adjust the pH to around 6 and form a gel-like precursor which was dispersed in distilled water and separated by centrifugation at 5000 rpm for 15 minutes. The washing and centrifugation was repeated at least 3 times to remove unreacted ions. The centrifuged product, in which the Si is assumed to be 12.5 mmol/L, was suspended in distilled water, nitric acid solution (1.0 mol/L) was added and stirred to adjust the pH to approximately 4. The suspension was sealed in a Teflon-lined stainless steel autoclave (50 mL) and heated at 100 °C for 48 h to give a transparent suspension from which the imogolite was precipitated by adding 28% ammonia solution. Finally, the precipitated samples were separated by centrifuging (6000 rpm for 30 min), washed with distilled water several times and dried at 80 °C for 1 day.

2.3. Preparation of Cu(II)-Grafted TiO₂

The Cu(II)-grafted TiO₂ photocatalyst was prepared by the impregnation method as previously described [53], using CuCl₂·2H₂O as the source of Cu(II). TiO₂ powder (1.0 g; 1.25×10^{-2} mol) was dispersed in 10 mL of distilled water.

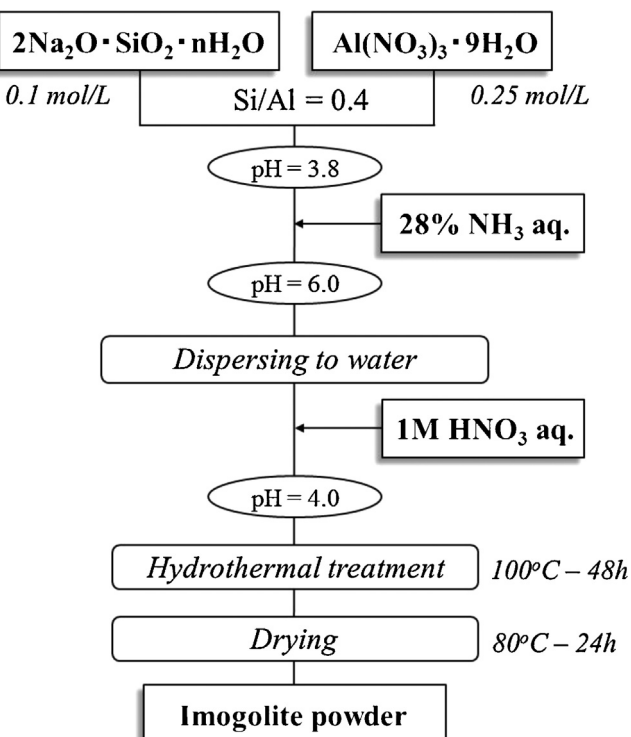


Fig. 1. Synthesis flowchart of imogolite powder by the hydrothermal method.

CuCl₂·2H₂O was weighed so that the weight fraction of Cu relative to TiO₂ was 1.0×10^{-3} (i.e., molar ratio of Cu/TiO₂ = 0.13). The CuCl₂·2H₂O was then added to the aqueous TiO₂ suspension and heated at 90 °C for 1 h with stirring in a vial reactor. The powder samples were separated from the suspension by centrifuging (6000 rpm for 30 min), washed with distilled water, dried at 110 °C for 24 h and finely ground using an agate mortar.

2.4. Preparation of Imogolite and TiO₂ or Cu(II)-Grafted TiO₂ Composites

The synthesized imogolite powders were dried at 80 °C for 2 days in a vacuum oven to remove the surface adsorbed water. The imogolite powder and TiO₂ or Cu(II)-grafted TiO₂ photocatalyst were then mixed using an agate mortar. The mixed mass ratios were as follows; TiO₂:imogolite = 1:0, 1:0.5, 1:1, 1:2, 1:3, 1:4, and Cu(II)-grafted TiO₂: imogolite = 1:0, 1:1, 3. The samples with different mixed mass ratio are denoted in this report as “TiO₂ X-im” and “Cu-TiO₂ X-im” (X indicates mixed mass ratio of imogolite).

2.5. Characterization

The crystalline phase in the samples was identified using a powder X-ray diffractometer (XRD, RINT2100; Rigaku, Japan) with monochromated Cu Kα radiation. The applied voltage and current to the Cu target was 40 kV–40 mA. IR spectroscopy was performed using a Fourier transform infrared spectrometer (FT-IR, JIR-7000; JEOL, Japan). The surface microstructures of the samples were examined by field emission-scanning electron microscopy (FE-SEM, S-4800; Hitachi, Japan) using an acceleration voltage of 5 kV. The morphology of the samples was investigated using TEM (HF-2000; Hitachi, Japan) operating at 200 kV. The samples for TEM were prepared by dispersing one drop of the sample in water and depositing on an amorphous carbon grid. To characterize the local structure around the Si⁴⁺ and Al³⁺ in the samples, the ²⁹Si and ²⁷Al solid state MASNMR spectra were acquired using a solid-state NMR

spectrometer (Bruker Avance II-500 spectrometer; Bruker BioSpin, Germany). The ^{29}Si MAS NMR data were acquired at 11.7 T (Lamor frequency of 99.926 MHz) using a 5 mm Doty MAS probe spun at 5–6 kHz; single-pulse excitation using $6\ \mu\text{s}$ ($\pi/10$) pulse widths and a recycle delay of 30 s. The spectra were referenced to tetramethyl silane (TMS). The ^{27}Al measurements were made at 11.7 T using a 4 mm Doty MAS probe spun at 10–12 kHz with a 1 s ($\pi/10$ pulse for solution) and a 1 s delay. The spectra were referenced to $\text{Al}(\text{H}_2\text{O})_6^{3+}$. The specific surface area and adsorption-desorption isotherms of the samples were measured by the N_2 gas adsorption BET method (Gemini V, Shimadzu, Japan). The samples were preheated in vacuo at 200 °C for 1 h. The measured experimental partial pressure (P/P_0) range was from 0.05 to 0.9. The water vapor adsorption-desorption isotherms were measured with a BELSORP-18 instrument (BEL, Japan) at 25 °C. The samples were preheated in vacuo at 200 °C for 20 h. The measured experimental partial pressure (P/P_0) range was from 0.05 to 0.9.

2.6. Evaluation of photocatalytic activity

The degradation of gaseous acetaldehyde (CH_3CHO) was carried out at room temperature in a batch-type reactor on the powder samples. This reaction temperature is higher than the boiling point of pure acetaldehyde (approximately 20 °C). The vessel was made of Pyrex glass, with a volume of 500 mL. Before photodegradation, the samples were irradiated in air using UV light (1.0 mW/cm²) for 2 days to clear the ubiquitous organic pollutants from the surface. The powder samples (0.05 g) were placed in the reaction vessel. Commercially available pure air was humidified to 6, 30, 50, and 80%RH by flowing through a water/ice mixture, and introduced to the reaction vessel at room temperature. A measured quantity of reaction gas (acetaldehyde gas; 4.5 μmol (200 ppm)) was then introduced into the reaction vessel using a Pressure-Lok® precision analytical syringe. After adsorption equilibration in the dark for 2 h, the reactor was placed below a UV light lamp (FL10BLB, Toshiba, Japan) or a fluorescent light lamp (FL10, Toshiba, Japan). In the latter case, a filter (<400 nm, CLAREX N-113; Nitto Jushi Kogyo, Japan) was used due to cut the wavelength to the UV range. The UV or fluorescent light intensity was 1.0 mW/cm² or 9500 lx, respectively. The decrease in acetaldehyde concentration and increase in CO_2 concentration was monitored using gas chromatography with nitrogen as the carrier gas (GC-8A; Shimadzu, equipped with a 2 m Porapak-Q column ZP-17 and a flame ionization detector).

3. Results and discussion

The TEM images of the synthetic imogolite sample (Fig. 2) shows the form of the sample to be fibrous tube bundles, each containing many individual tubes of ca. 3–5 nm OD, corresponding to imogolite. Natural imogolite typically contains web-like structures, and a single-walled aluminosilicate nanotubular mineral imogolite has an OD of 2.2 nm and an ID of ~1.0 nm [45]. Thus, the synthetic sample has a slightly larger OD than natural imogolite. Single-walled nanotubular aluminosilicate imogolite is difficult to determine by X-ray diffraction because of its small tube size. The XRD pattern of the synthetic sample appears almost amorphous, with a broad peak at $2\theta = 40^\circ$ (see Figure S1 in the Supporting Information). This broad peak is attributed to gibbsite ($\text{Al}(\text{OH})_3$). The structure of the imogolite has been well characterized in a number of previous studies [45]. The nanotube wall consists of a curved gibbsite [$\text{Al}(\text{OH})_3$] sheet with orthosilicate groups [O_3SiOH] attached to the inner wall, resulting in the empirical formula $(\text{OH})_3\text{Al}_2\text{O}_3\text{SiOH}$ [55]. It is thought that the synthetic sample is nanotubular imogolite partly covered by gibbsite.

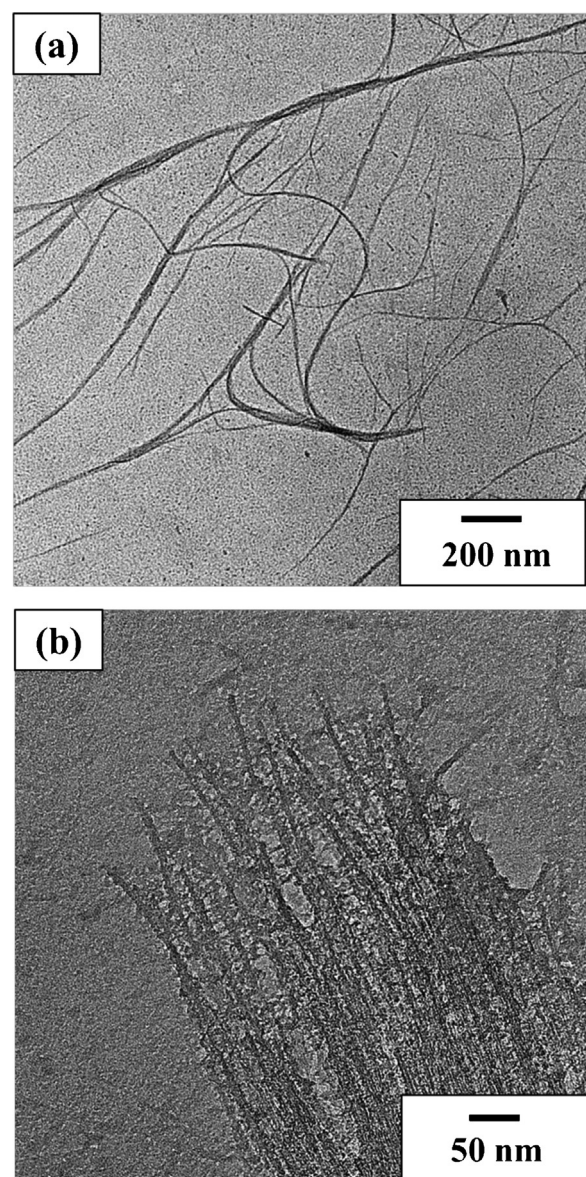


Fig. 2. TEM images of the imogolite sample synthesized by the hydrothermal method. (a) large area, (b) high resolution.

Fig. 3 shows the ^{27}Al and ^{29}Si NMR spectra of the sample. The ^{27}Al NMR spectrum of the sample has a resonance with a chemical shift of 6 ppm, characteristic of the octahedrally-coordinated Al(VI) polymerized in the gibbsite-like layer [56]. This chemical shift corresponds to the Al arrangement in imogolite [57]. Other small peaks at about 38 and 63 ppm have been suggested by MacKenzie et al. [58,59] to arise from Al in slightly different tetrahedral environments, although the peak at about 38 ppm could possibly have been due to a more regular 5-coordinated Al site [60,61]. The amount of Al in these two sites attributed to 4 and 5-coordinated Al is very low. The ^{29}Si NMR spectrum of the sample exhibits a main resonance at -78 ppm. This chemical shift is typical of the imogolite structure and originates from Si in a Q^0 site bonded to one OH group [51,62]. A shoulder appearing at about -86 ppm eventually becomes the broad resonance of the fully dehydroxylated phase [63]. These results indicate that each Si is attached through oxygen to six octahedral Al atoms, and each Al is attached through oxygen to three Si atoms. The local environment of Si and Al in the synthetic sample is characteristic of an imogolite-type configuration at the molecular scale.

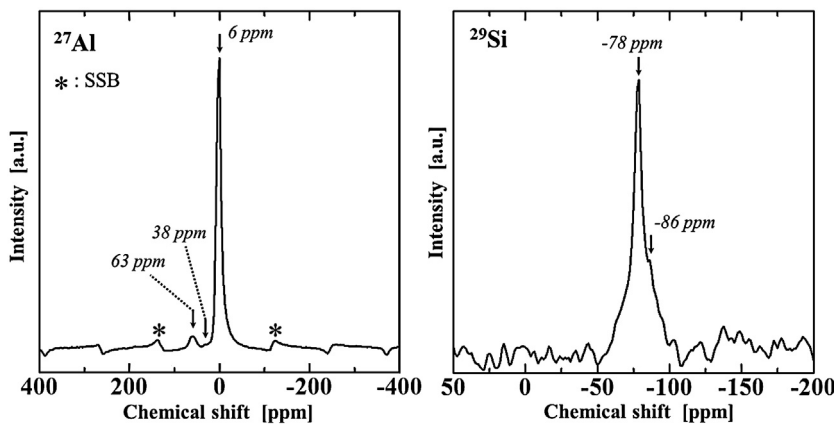


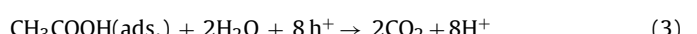
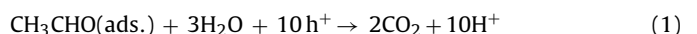
Fig. 3. 11.7 T ^{27}Al and ^{29}Si MAS NMR spectra of the sample synthesized by the hydrothermal method. Left: ^{27}Al , right: ^{29}Si .

Nitrogen and water vapor adsorption–desorption isotherms of the synthetic sample are shown in Fig. 4. The nitrogen isotherm shows type I behavior, indicating the presence of micropores, with small hysteresis loops due to limited external mesoporosity, most probably derived from slit-shaped mesopores among the fiber bundles [64]. In contrast, the water vapor adsorption behavior increases with increasing P/P_0 but the desorption line does not close. This is attributed to water molecules adsorbed on the sample surface which cannot desorb. The surface of imogolite is covered by hydroxyl groups [45], and the IR spectrum shows that these hydroxyl groups are located on the surface of the synthetic imogolite (see Figure S2 in the Supporting Information). It is probable that the water molecules adsorbed on the sample surface cannot easily desorb because of the hydrogen bonding between the water molecules and surface hydroxyl groups. The specific surface areas (SSA) were 245 and 509 m^2/g for nitrogen and water vapor, respectively. The SSA derived from the nitrogen measurement is similar to that of synthetic imogolite [50,51] but the SSA calculated from the water vapor measurement is larger than for nitrogen, reflecting the strong affinity of the sample for water molecules. These results indicate a successful imogolite synthesis.

Fig. 5 shows the SEM images of the TiO_2 -imogolite composites. The **TiO₂ 0.5-imolite** sample has TiO_2 particles with the size of 100–300 nm, and a grain-like morphology with polygonal grain shapes. There are white shapes under the TiO_2 particles, and those are imogolite. In the other composite samples, with increasing the content of imogolite, imogolite was found to cover the TiO_2 particle surfaces, and the area covered by imogolite increases on the TiO_2 surface in the **TiO₂ 3-imolite** and **TiO₂ 4-imolite** samples. In the **TiO₂ 4-imolite** sample, some of TiO_2 particles are entirely covered in part

by the imogolite (Fig. 5(f)). Although the TiO_2 particles are partly agglomerated, they are near the imogolite in the **TiO₂ 2-imolite**, **TiO₂ 3-imolite**, and **TiO₂ 4-imolite** samples.

Fig. 6 shows the results of acetaldehyde (CH_3CHO) degradation under UV light irradiation at various relative humidities in the presence of the imogolite, TiO_2 , and TiO_2 -imogolite composite samples mixed in various ratios. When UV light is irradiated to the vessel without samples, concentration of acetaldehyde does not change. In the case of **imogolite**, concentration of acetaldehyde decreases compared to initial acetaldehyde concentration because acetaldehyde is adsorbed on the imogolite surface (Fig. 6(a)). However, the concentration change does not occur under UV light irradiation. This is because imogolite cannot exhibit photocatalytic activity under UV light irradiations although **imogolite** absorbs UV light (Figure S4). The degree of degradation of acetaldehyde depends on the catalyst and the relative humidity. On exposure to UV light, the acetaldehyde concentrations decrease. In the presence of the TiO_2 photocatalyst the oxidative photodegradation of acetaldehyde proceeds as follows [65]:



where h^+ is a hole generated by the photoinduced charge separation in TiO_2 . One acetaldehyde molecule decomposes into two CO_2 molecules, which is the final product. Prior to UV irradiation, the acetaldehyde concentration of all the samples decreased below the initial acetaldehyde concentration, this effect becoming more marked with increasing the imogolite content of the

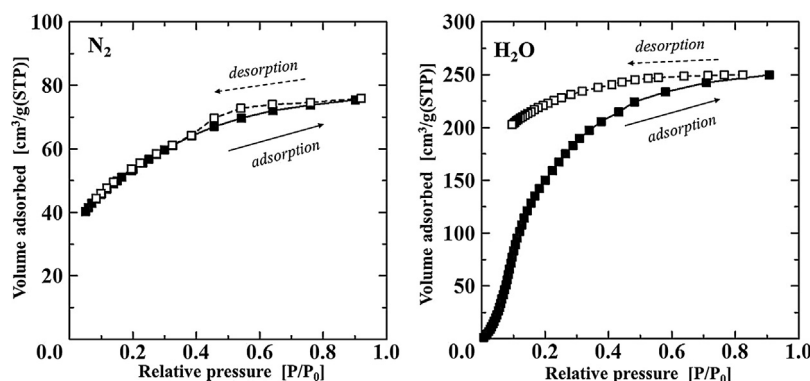


Fig. 4. Nitrogen (N_2) and water vapor (H_2O) adsorption–desorption isotherms of the sample synthesized by the hydrothermal method. Left: N_2 , right: H_2O . Full symbols: adsorption branch; open symbols: desorption branch.

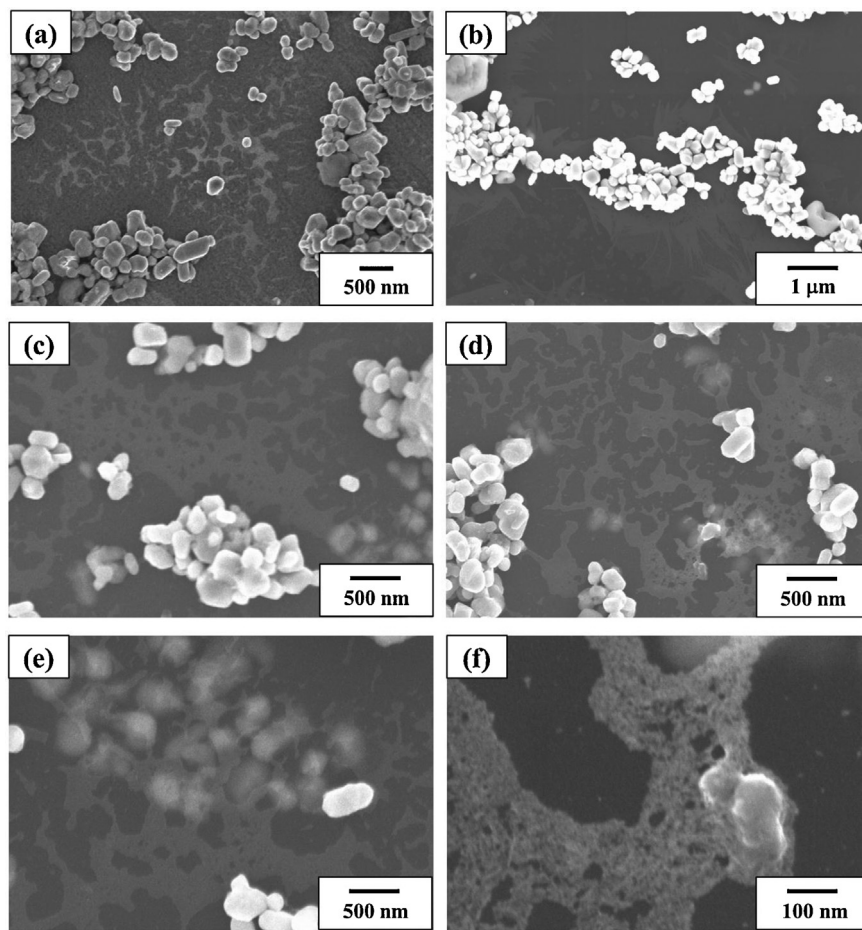
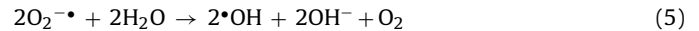


Fig. 5. SEM images of the TiO₂-imogolite composites; (a) TiO₂ 0.5-imo, (b) TiO₂ 1-imo, (c) TiO₂ 2-imo, (d) TiO₂ 3-imo, (e) TiO₂ 4-imo, (f) enlarged image in the TiO₂ 4-imo sample.

samples. This result indicates that the imogolite plays an important role as an adsorbent. The decrease in the acetaldehyde concentration increased at lower relative humidities. Since the surface of the TiO₂ and imogolite is hydrophilic, more water molecules are adsorbed on the surface at higher relative humidity. As a result, adsorption of the acetaldehyde on the TiO₂ and imogolite surfaces is impeded under higher relative humidities. After UV irradiation, the decrease in the acetaldehyde concentration becomes high, due to the photodegradation of the acetaldehyde by the TiO₂ photocatalyst. In the case of **TiO₂ 0-imo**, the photodegradation of acetaldehyde was higher at lower relative humidity (Fig. 6(b)). Zhang et al. [66] reported that the photocatalytic degradation efficiencies of carbonyl compounds decreased slightly with an increase in relative humidity at the lower humidity range. This experimental result may be due to the competitive adsorption between water molecules and the molecules of carbonyl compounds on the photocatalyst surface, and the masking of moisture on the active sites of the photocatalyst surface. However, the photodegradation rate of acetaldehyde at 30 and 50%RH was higher than that at 6%RH, and this tendency is also shown by the TiO₂-imogolite composite samples (Fig. 6(c)–(g)). Hydroxyl radicals are known to be strong oxidants, contributing to the degradation of the acetaldehyde in the presence of water vapor. The water molecules can be transformed into hydroxyl radicals ($\cdot\text{OH}$) by reaction with the photogenerated holes (h^+) or superoxide radicals ($\text{O}_2^{\cdot-}$) at the photocatalyst surface via the following reactions [67]:



As described in reactions (1)–(5), the moderate water molecules are required to degrade the acetaldehyde although the competitive adsorption between water molecules and the acetaldehyde molecules is also a factor. The TiO₂-imogolite composite samples exhibited higher activity in the photodegradation of acetaldehyde than **TiO₂ 0-imo** because the adsorbed acetaldehyde is decomposed not only on the TiO₂ but also on the imogolite. The active oxygen species such as $\cdot\text{OH}$, $\text{O}_2^{\cdot-}$, and H_2O_2 generated on the TiO₂ surface are released [66–70], diffusing through the gas phase and oxidizing the acetaldehyde.

Fig. 7 shows the CO₂ generation rate of the TiO₂ and TiO₂-imogolite composite samples at various relative humidities under UV irradiation. In all samples, CO₂ is generated by UV irradiation, indicating that acetaldehyde is decomposed by the TiO₂ photocatalyst into CO₂, the final product (Figure S3). The CO₂ generation rate of the TiO₂-imogolite composite samples increases over that of **TiO₂ 0-imo**, and the rate is higher with an increase in the imogolite content up to sample **TiO₂ 3-imo**. Acetaldehyde adsorbed on the TiO₂ and imogolite surfaces is decomposed into CO₂ by the TiO₂ photocatalyst. However, the CO₂ generation rate of **TiO₂ 4-imo** is lower, because some of TiO₂ particles are entirely covered in part by the imogolite, and the UV light is prevented from being irradiated onto the TiO₂ surface by the increased coverage by the imogolite (Figure S4). **TiO₂ 2-imo** and **TiO₂ 3-imo** exhibited higher CO₂ generation rates at various relative humidities. These results suggest that optimum content of a combination of TiO₂ as

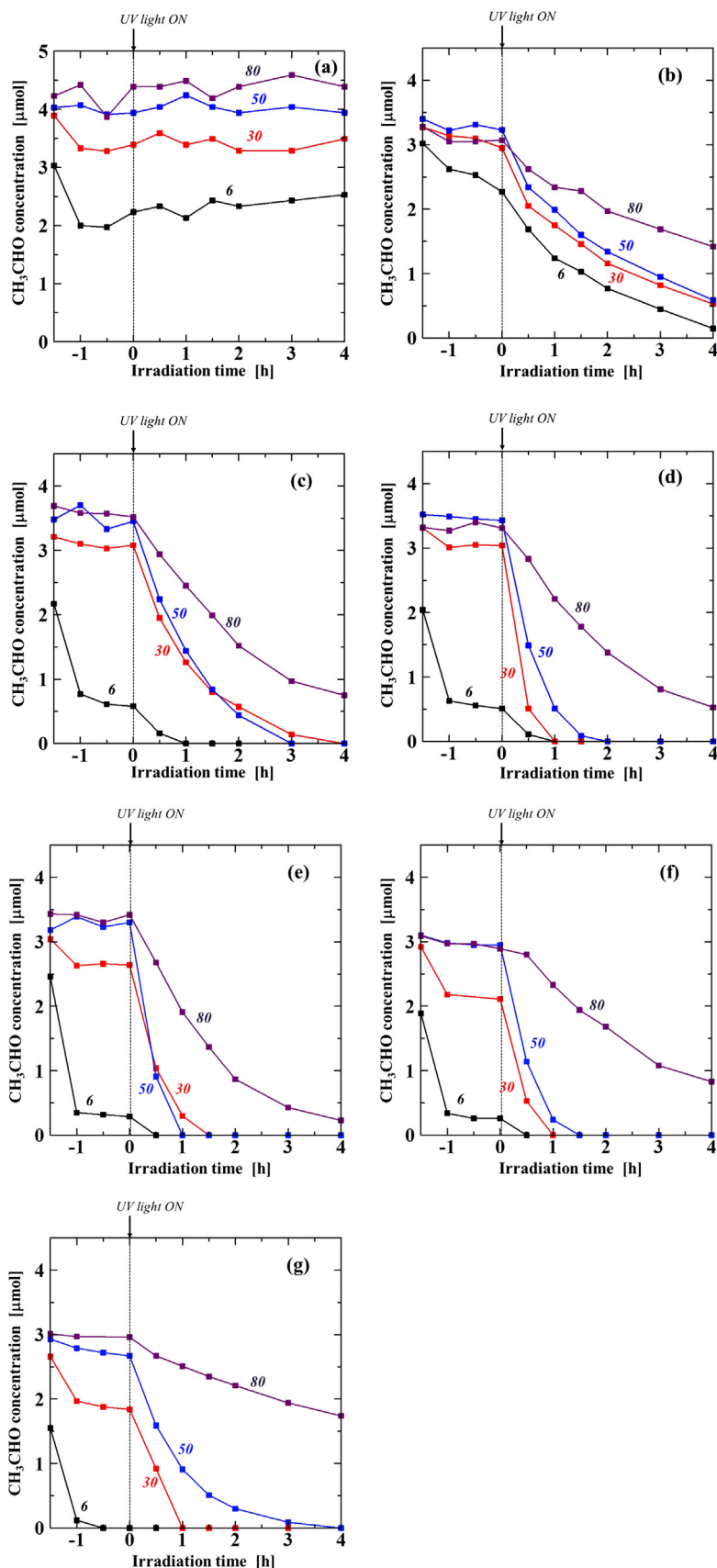


Fig. 6. Change in acetaldehyde concentrations as a function of UV light irradiation time in the presence of the TiO_2 –imogolite composites under various relative humidities; (a)Imogolite, (b) TiO_2 0-imolite, (c) TiO_2 0.5-imolite, (d) TiO_2 1-imolite, (e) TiO_2 2-imolite, (f) TiO_2 3-imolite, (g) TiO_2 4-imolite. The color of the line indicates the relative humidity; black: 6, red: 30, blue: 50, and purple: 80%RH (For interpretation of the references to colour in this figure legend, the reader is referred to the web version of this article.)

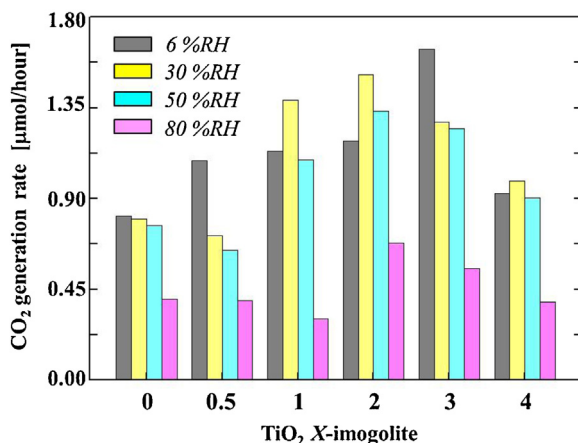
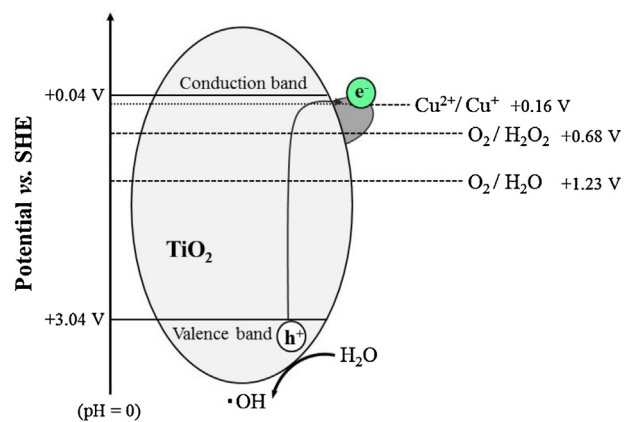


Fig. 7. CO₂ generation rate of the TiO₂ and TiO₂–imogolite composites under various relative humidities.

the photocatalyst and imogolite as the adsorbent produce a useful material for the degradation of acetaldehyde.

Fig. 8 shows the results of acetaldehyde (CH₃CHO) visible light degradation at various relative humidities in the presence of the Cu(II)-grafted TiO₂ and Cu(II)-grafted TiO₂–imogolite composite samples, the latter mixed in Cu(II)-grafted TiO₂:imogolite = 1:3 mass ratio. In UV-vis spectrum of **Cu-TiO₂ 0-imo**, it shows absorption at 600–800 nm (Figure S4). The absorption at 600–800 nm can be assigned to the Cu(II) d-d transition [53], indicating that Cu(II) is grafted on the TiO₂ surface. In the case of the imogolite, which was not included with Cu(II)-grafted TiO₂, the results of the acetaldehyde concentration change under visible light were almost the same as the results under UV light. Prior to the irradiation with visible light, the acetaldehyde concentration of **Cu-TiO₂ 0-imo** decreased slightly due to absorption on the TiO₂ surface (Fig. 8(a)). However, this decrease was smaller than with **TiO₂ 0-imo** (Fig. 6(b)). It is presumed that the Cu²⁺ ions are absorbed on the active sites of the TiO₂ surface. In contrast, the acetaldehyde concentration of **Cu-TiO₂ 3-imo** (Fig. 8(b)) decreases by about the same amount as **TiO₂ 3-imo** (Fig. 6(f)), and the decrease of acetaldehyde in **Cu-TiO₂ 3-imo** is higher than that for **Cu-TiO₂ 0-imo**. After visible light irradiation, the acetaldehyde concentration of **Cu-TiO₂ 0-imo** gradually decreases, attributed to the photodegradation of the acetaldehyde by the Cu(II)-grafted TiO₂ photocatalyst. This photodegradation rate increases at higher relative humidities.



Scheme 1. Mechanism of photocatalytic activity under visible light. Visible light irradiation induces interfacial charge transfer from the valence band of TiO₂ to the Cu(II) ion [53].

The photodegradation rate of **Cu-TiO₂ 3-imo** also becomes greater at higher relative humidities. These trends are different from those of **TiO₂ 0-imo** and **TiO₂ 3-imo** (Fig. 6(b) and (f)).

Cu(II)-grafted TiO₂ is sensitive to visible light. In this system, it is suggested photoinduced interfacial charge transfer (IFCT) occurs between the continuous energy levels of solids and the discrete levels of the molecular species on the surface. That is, electrons in the valence band (VB) of the TiO₂ are transferred directly to Cu(II), forming Cu(I). The holes produced in the VB are capable of directly decomposing organic substances or generating hydroxyl radicals (•OH) by reacting with the water molecules (Scheme 1) [53,54,71]. The reduction reaction mechanism may possibly proceed by multielectron reduction [72]:

Two-electron reduction



Four-electron reduction



Consequently, this system functions catalytically and exhibits oxidative decomposition activity. In this IFCT model, water molecules play an important role in generating hydroxyl radicals and reducing oxygen (multielectron reduction). In addition, the hydroxyl radicals and hydrogen peroxide formed by two-electron

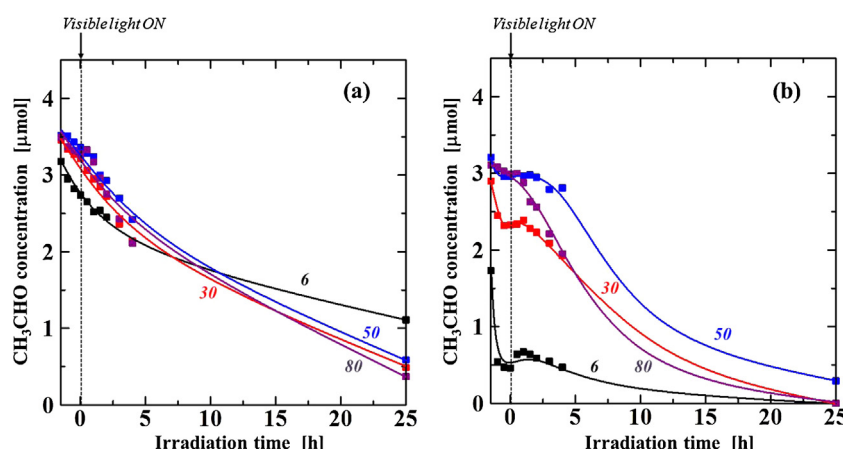
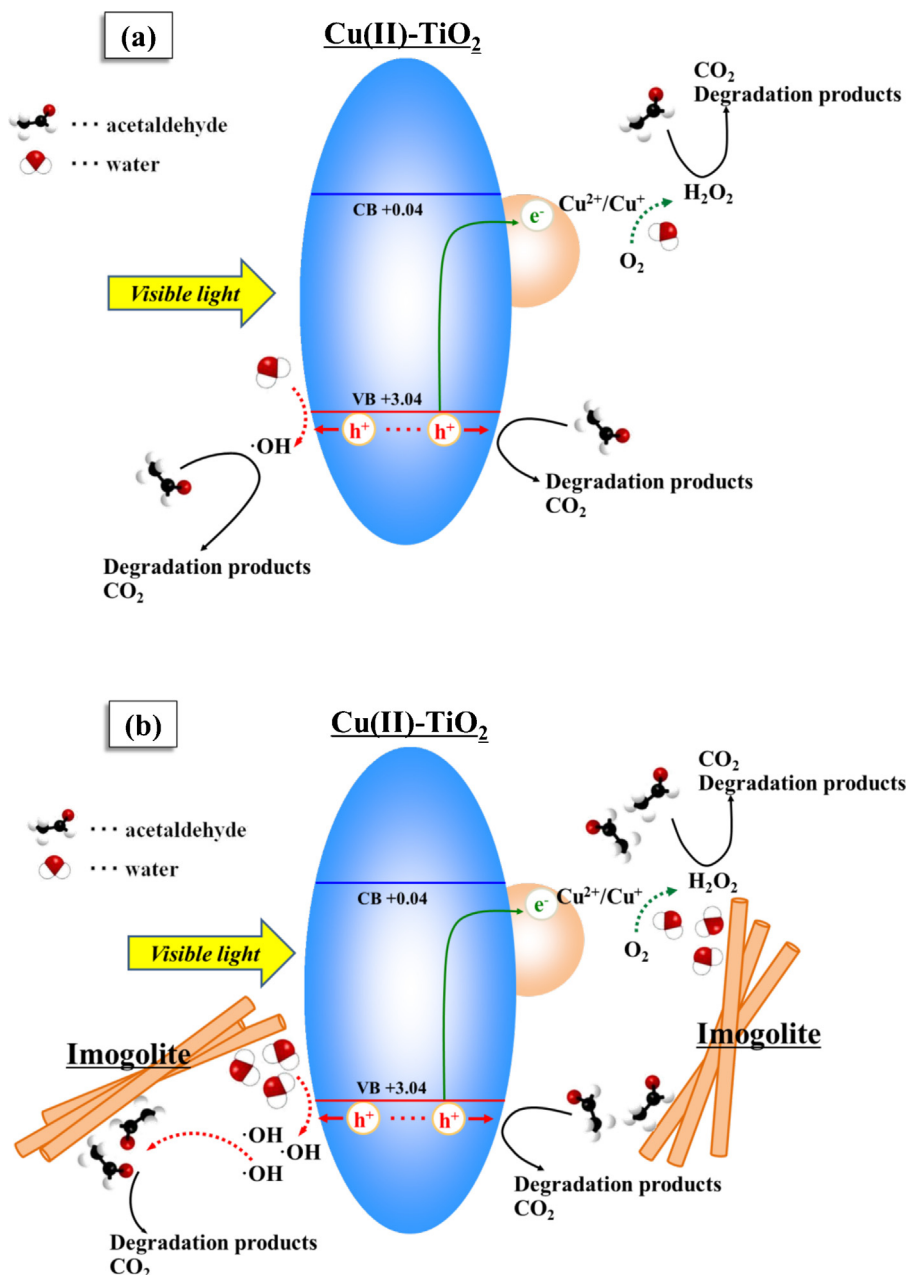


Fig. 8. Change in acetaldehyde concentrations as a function of visible light irradiation time in the presence of the Cu(II)-grafted TiO₂ and Cu(II)-grafted TiO₂–imogolite composites under various relative humidities; (a) **Cu-TiO₂ 0-imo**, (b) **Cu-TiO₂ 3-imo**. The color of line indicates the relative humidity; black: 6, red: 30, blue: 50, and purple: 80%RH (For interpretation of the references to colour in this figure legend, the reader is referred to the web version of this article.)



Scheme 2. Possible photodegradation mechanisms of acetaldehyde under visible light irradiation; (a)Cu(II)-grafted TiO₂, (b)Cu(II)-grafted TiO₂-imogolite composite.

reduction are strongly oxidizing and can decompose most organic compounds (**Scheme 2(a)**).

Fig. 9 shows the CO₂ generation rate of the **Cu-TiO₂** and **Cu-TiO₂-3-im** samples at various relative humidities under visible light irradiation. In both samples, CO₂ was generated by visible light irradiation (Figure S5), indicating that acetaldehyde was decomposed into CO₂ by the Cu(II)-grafted TiO₂ photocatalyst. The CO₂ generation rate of **Cu-TiO₂-3-im** is greater than that of **Cu-TiO₂**. But both samples show similar photodegradation of acetaldehyde (**Fig. 8(a)** and (**b**)). It is suggested that imogolite adsorbs not only acetaldehyde but also the intermediate products (CH₃COOH) during the decomposition of acetaldehyde and these are then decomposed to CO₂ by the radical species generated on the Cu(II)-grafted TiO₂ surface (**Scheme 2(b)**). The CO₂ generation rate in both samples becomes greater at higher relative humidities because water molecules are implicated in the generation of many of the radical species.

In the case of the TiO₂ photocatalyst, the CO₂ generation rate decreases at higher relative humidities, and this effect is variable (**Fig. 7**), indicating the need for the reaction environment to be taken into consideration in any application. In contrast, the CO₂ generation rate of the Cu(II)-grafted TiO₂ photocatalyst was less affected by relative humidity. These results are interesting because this is the first report of the effect of the relative humidity on the photocatalytic activity of Cu(II)-grafted TiO₂, an IFCT type photocatalyst. We believe this to be a very important result because it exhibits photocatalytic activity under a variety of environments, in particular the UV and visible (fluorescent) photocatalytic activity of Cu(II)-grafted TiO₂. In addition, the present Cu(II)-grafted TiO₂ – imogolite composite exhibits very efficient absorption ability and photodecomposition of acetaldehyde under visible light. This suggests that these results should usefully expand the applications of the Cu(II)-grafted TiO₂.

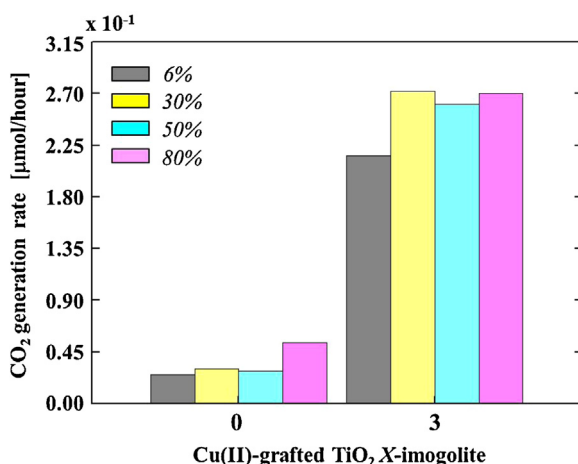


Fig. 9. CO₂ generation rate of the Cu(II)-grafted TiO₂ and Cu(II)-grafted TiO₂-imogolite composites under various relative humidities.

4. Conclusions

Imogolite with a nanotubular structure was synthesized hydrothermally and used to prepare imogolite-TiO₂ and imogolite-Cu(II)-grafted TiO₂ composites. The photocatalytic degradation of acetaldehyde by these compounds was investigated. Nanotubular imogolite had a high specific surface area (245 m²/g), with a strong surface affinity for water molecules. Under UV irradiation, photodegradation of acetaldehyde by the imogolite-TiO₂ composite was greater than that of TiO₂, indicating that imogolite plays an important role in adsorbing the acetaldehyde. The optimum mixtures of the TiO₂ as the photocatalyst and imogolite as the adsorbent lie between the compositions **TiO₂ 2-imo** and **TiO₂ 3-imo**. However, the photoactivity is also dependent on the relative humidity. With increasing relative humidity, the photodegradation activity decreases, but the photodegradation activity of the Cu(II)-grafted TiO₂-imogolite composite of composition **Cu-TiO₂ 3-imo** was less affected by the relative humidity, and this composite also exhibited higher photoactivity under visible light irradiation than Cu(II)-grafted TiO₂ (**Cu-TiO₂**). The present imogolite-containing composite is suggested to be a very effective visible-light-driven photocatalyst and could be used to completely decompose or remove VOCs.

Acknowledgments

The authors are grateful to Dr. M. Suzuki (National Institute of Advanced Industrial Science and Technology, Japan) for helpful discussion about the synthesis of imogolite. The authors are grateful to Prof. Y. Kitamoto (Tokyo Institute of Technology, Japan) for the TEM, to Prof. T. Akatsu (Tokyo Institute of Technology, Japan) for the XRD, to Prof. T. Yamaguchi and Dr. H. Tabata (Tokyo Institute of Technology, Japan) for the SEM, to Prof. Y. Kameshima (Okayama University, Japan) for the measurement of water vapor adsorption-desorption isotherms, to Ms. H. Tokimori (Tokyo Institute of Technology, Japan) for the helpful support of the SEM observation, and to Ms. T. Nomura (Kanagawa Academy of Science and Technology, Japan) for the helpful support of the evaluation in the photocatalytic activity.

Appendix A. Supplementary data

Supplementary data associated with this article can be found, in the online version, at <http://dx.doi.org/10.1016/j.apcatb.2013.03.0041>.

References

- R.M. Alberici, W.E. Jardim, *Applied Catalysis B: Environmental* 14 (1997) 55–68.
- R. Beauchet, P. Magnoux, J. Mijoin, *Catalysis Today* 124 (2007) 118–123.
- H. Jorio, K. Kiared, R. Brzezinski, A. Leroux, G. Viel, M. Heitz, *Journal of Chemical Technology & Biotechnology* 73 (1998) 183–196.
- M.P. Cal, M.J. Rood, S.M. Larson, *Gas Separation & Purification* 10 (1996) 117–121.
- F. Delage, P. Pré, P.L. Cloirec, *Environmental Science & Technology* 34 (2000) 4816–4821.
- K. Everaert, J. Baeyens, J. Degrève, *Journal of the Air & Waste Management Association* 52 (2002) 1378–1388.
- C.L. Chuang, P.C. Chiang, E.E. Chang, *Chemosphere* 53 (2003) 17–27.
- L. Fournel, P. Mochon, J.L. Fanlo, P.L. Cloirec, *Environmental Technology* 26 (2005) 1277–1287.
- K.-J. Kim, C.-S. Kang, Y.-J. You, M.-C. Chung, M.-W. Woo, W.-J. Jeong, N.-C. Park, H.-G. Ahn, *Catalysis Today* 111 (2006) 223–228.
- S. Giraudet, P. Pré, H. Tezel, P.L. Cloirec, *Carbon* 44 (2006) 1873–1883.
- A. Fujishima, T.N. Rao, D.A. Tryk, *Journal of Photochemistry and Photobiology C: Photochemistry Reviews* 1 (2000) 1–21.
- T. Kawai, T. Sakata, *Nature* 286 (1980) 474–476.
- Y. Ohko, D.A. Tryk, K. Hashimoto, A. Fujishima, *Journal of Physical Chemistry B* 102 (1998) 2699–2704.
- I. Nakamura, N. Negishi, S. Katsuna, T. Ihara, S. Sugihara, K. Takeuchi, *Journal of Molecular Catalysis A: Chemical* 161 (2000) 205–212.
- M.C. López, M.I. Fernández, S. Rodríguez, J.A. Santaballa, S. Steenken, E. Vulliet, *ChemPhysChem* 6 (2005) 2064–2074.
- M. D'Arienzo, M. Crippa, A.A. Essawy, R. Scotti, L. Wahba, F. Morazzoni, P. Gentile, I.R. Bellobono, S. Polozzi, *Journal of Physical Chemistry C* 114 (2010) 15755–15762.
- M.A. Henderson, N.A. Deskins, R.T. Zehr, M. Dupuis, *Journal of Catalysis* 279 (2011) 205–212.
- K. Sunada, Y. Kukuchi, K. Hashimoto, A. Fujishima, *Environmental Science & Technology* 32 (1998) 726–728.
- K. Sunada, T. Watanabe, K. Hashimoto, *Environmental Science & Technology* 37 (2003) 4785–4789.
- K. Sunada, T. Watanabe, K. Hashimoto, *Journal of Photochemistry and Photobiology A: Chemistry* 156 (2003) 227–233.
- A. Vohra, D.Y. Goswami, D.A. Deshpande, S.S. Block, *Journal of Industrial Microbiology and Biotechnology* 32 (2005) 364–370.
- K.L. Yeung, W.K. Leung, N. Yao, S. Cao, *Catalysis Today* 143 (2009) 218–224.
- J. Chen, M. Liu, L. Zhang, J. Zhang, L. Jin, *Water Research* 37 (2003) 3815–3820.
- D. Zhang, G. Li, J.C. Yu, *Journal of Materials Chemistry* 20 (2010) 4529–4536.
- Y.-J. Xu, Y. Zhuang, X. Fu, *Journal of Physical Chemistry* 114 (2010) 2669–2676.
- J. Schwitzgebel, J.G. Ekerdt, H. Gerischer, A. Heller, *Journal of Physical Chemistry* 99 (1995) 5633–5638.
- P.A. Kolinko, D.V. Kozlov, A.V. Vorontsov, S.V. Preis, *Catalysis Today* 122 (2007) 178–185.
- L. Zhang, W.A. Anderson, S. Sawell, C. Moralejo, *Chemosphere* 68 (2007) 546–553.
- A.T. Hodgson, H. Destaillats, D.P. Sullivan, W.J. Fisk, *Indoor Air* 17 (2007) 305–316.
- J. Auvinen, L. Wirtanen, *Atmospheric Environment* 42 (2008) 4101–4112.
- M.E. Zorn, S.O. Hay, M.A. Anderson, *Applied Catalysis B: Environmental* 99 (2010) 420–427.
- K. Sekiguchi, W. Morinaga, K. Sakamoto, H. Tamura, F. Yasui, M. Mehrjouei, S. Müller, D. Möller, *Applied Catalysis B: Environmental* 97 (2010) 190–197.
- Y. Zhang, Z.-R. Tang, X. Fu, Y.-J. Xu, *ACS Nano* 4 (2010) 7303–7314.
- H. Yoneyama, S. Haga, S. Yamana, *Journal Physical Chemistry* 93 (1989) 4833–4837.
- T. Kaneko, H. Shimotsuma, M. Kajikawa, T. Hatamachi, T. Kodama, Y. Kitayama, *Journal of Porous Materials* 8 (2001) 295–301.
- K. Mogyorósi, A. Farkas, I. Dékány, I. Ilisz, A. Domki, *Environmental Science & Technology* 36 (2002) 3618–3624.
- K. Mogyorósi, I. Dékány, J.H. Fendler, *Langmuir* 19 (2003) 2938–2946.
- C. Ooka, H. Yoshida, K. Suzuki, T. Hattori, *Chemistry Letters* 32 (2003) 896–897.
- C. Ooka, H. Yoshida, K. Suzuki, T. Hattori, *Applied Catalysis A: General* 260 (2004) 47–53.
- R. Kun, K. Mogyorósi, I. Dékány, *Applied Clay Science* 32 (2006) 99–110.
- J. Ménesi, L. Körösi, E. Bazsó, V. Zöllmer, A. Richardt, I. Dékány, *Chemosphere* 70 (2008) 538–542.
- A. Nikolopoulou, D. Papoulis, S. Komameni, P. Tsolis-Katagas, D. Panagiotaras, G.H. Kacandes, P. Zhang, S. Yin, T. Sato, *Applied Clay Science* 46 (2009) 363–368.
- Y. Kameshima, Y. Tamura, A. Nakajima, K. Okada, *Applied Clay Science* 45 (2009) 20–23.
- D. Kabanova, M. Trejo, H. Destaillats, J. Cervini-Silva, *Applied Clay Science* 42 (2009) 563–568.
- P.D.G. Cradwick, V.C. Farmer, J.D. Russell, C.R. Masson, K. Wada, N. Yoshinaga, *Nature Physical Science* 240 (1972) 187–189.
- K. Wada, N. Yoshinaga, *American Mineralogist* 54 (1969) 50–71.
- V.C. Farmer, A.R. Fraser, J.M. Tait, *Journal of the Chemical Society, Chemical Communication* (1977) 462–463.
- V.C. Farmer, B.F.L. Smith, J.M. Tait, *Clay Minerals* 14 (1979) 103–107.

- [49] S. Imamura, T. Kokubu, T. Yamashita, Y. Okamoto, K. Kajiwara, H. Kanai, *Journal of Catalysis* 160 (1996) 137–139.
- [50] W.C. Ackerman, D.M. Smith, J.C. Huling, Y.-M. Kim, J.K. Bailey, C.J. Brinker, *Langmuir* 9 (1993) 1051–1057.
- [51] F. Ohashi, S. Tomura, K. Akaku, S. Hayashi, S.-I. Wada, *Journal of Materials Science* 39 (2004) 1799–1801.
- [52] M. Suzuki, F. Ohashi, K. Inukai, M. Maeda, S. Tomura, T. Mizota, *Mineral Journal* 22 (2000) 1–10.
- [53] H. Irie, S. Miura, K. Kamiya, K. Hashimoto, *Chemical Physics Letters* 457 (2008) 202–205.
- [54] H. Irie, K. Kamiya, T. Shibanuma, S. Miura, D.A. Tryk, T. Yokoyama, K. Hashimoto, *Journal of Physical Chemistry C* 113 (2009) 10761–10766.
- [55] G.I. Yuçelen, R.P. Choudhury, A. Vyalikh, U. Scheler, H.W. Beckham, S. Nair, *Journal of American Chemical Society* 133 (2011) 5397–5412.
- [56] R.A. Kinsey, R.J. Kirkpatrick, J. Hower, K.A. Smith, E. Oldfield, *American Mineralogist* 70 (1985) 537–548.
- [57] S. Hiradate, H. Hirai, H. Hashimoto, *Geoderma* 136 (2006) 696–707.
- [58] K.J.D. MacKenzie, I.W.M. Brown, R.H. Meinhold, M.E. Bowden, *Journal of American Ceramic Society* 68 (1985) 266–272.
- [59] K.J.D. MacKenzie, I.W.M. Brown, R.H. Meinhold, M.E. Bowden, *Journal of American Ceramic Society* 68 (1985) 293–297.
- [60] L.B. Alemany, G.W. Kirker, *Journal of American Chemical Society* 108 (1986) 6158–6162.
- [61] M. Hatakeyama, T. Hara, N. Ichikuni, S. Shimazu, *Bulletin of the Chemical Society of Japan* 84 (2011) 656–659.
- [62] I. Jaymes, A. Douy, D. Massiot, J.-P. Busnel, *Journal of American Ceramic Society* 78 (1995) 2648–2654.
- [63] K.J.D. MacKenzie, M.E. Bowden, I.W.M. Brown, R.H. Meinhold, *Clays and Clay Minerals* 37 (1989) 317–324.
- [64] B. Bonelli, I. Bottero, N. Ballarini, S. Passeri, F. Cavani, E. Garrone, *Journal of Catalysis* 264 (2009) 15–30.
- [65] I. Sopyan, M. Watanabe, S. Murasawa, K. Hashimoto, A. Fujishima, *Journal of Photochemistry and Photobiology A: Chemistry* 98 (1996) 79–86.
- [66] M. Zhang, T. An, J. Fu, G. Sheng, X. Wang, X. Hu, X. Ding, *Chemosphere* 64 (2006) 423–431.
- [67] G. Vincent, P.M. Marquaire, O. Zahraa, *Journal of Hazardous Materials* 161 (2009) 1173–1181.
- [68] T. Tatsuma, W. Kubo, A. Fujishima, *Langmuir* 18 (2002) 9632–9634.
- [69] W. Kubo, T. Tatsuma, *Analytical Science* 20 (2004) 591–593.
- [70] W. Kubo, T. Tatsuma, A. Fujishima, H. Kobayashi, *Journal of Physical Chemistry B* 108 (2004) 3005–3009.
- [71] H. Yu, H. Irie, K. Hashimoto, *Journal of American Chemical Society* 132 (2010) 6898–6899.
- [72] A.J. Bard, R. Parsons, J. Jordan, *Standard Potentials in Aqueous Solution*, Marcel Dekker, New York, 1985, 49–66.